11th World Congress on Computational Mechanics (WCCM XI)
5th European Conference on Computational Mechanics (ECCM V)
6th European Conference on Computational Fluid Dynamics (ECFD VI)
E. Oñate, J. Oliver and A. Huerta (Eds)

A FEM MODEL FOR PREDICTION OF FATIGUE CRACK INITIATION IN FORGED M3:2 TOOL STEEL IN HIGH CYCLE FATIGUE

N. A. GIANG*, U. A. ÖZDEN*, A. BEZOLD* and C. BROECKMANN*

* Institute for Materials Application in Mechanical Engineering (IWM)
RWTH Aachen
Augustinerbach 4, D-52062 Aachen, Germany
e-mail: g.ngocanh@iwm.rwth-aachen.de, web page: http://www.iwm.rwth-aachen.de/

Key words: fatigue crack incubation, fatigue crack initiation, finite element method, high cycle fatigue, high speed tool steel.

Abstract. In general, failure of a component due to cyclic loading can be divided into 3 stages namely the fatigue crack incubation (i.e. formation of crack plus early crack growth), short crack, and long crack growth. The two consecutive stages, incubation and short crack growth, are also referred as fatigue crack initiation. It has been generally accepted that crack initiation occupies most of the fatigue life in HCF regime. For predicting the initiation life, a model combining two step simulation approaches including incubation life estimated by the Fatemi-Socie damage model and short crack life calculated by continuum damage mechanic (CDM) are used. The integrated CDM in FEM was done with VUMAT subroutine of ABAQUS/EXPLICIT. In this study, forged M3:2 high speed tool steel (DIN HS6-5-3) is applied to the validation of this proposed model. By estimating the cycles to the crack initiation the numerical model generates a useful tool for lifetime calculations.

1 INTRODUCTION

In industrial applications high speed tool steels are mainly used for cutting tool materials. These tools are always subjected by alternating loads, which come from vibrations of machines during cutting processes. Cutting tools are mostly failure by these types of loading.

In forged M3:2 tool steel at micro scale, primary and eutectic carbides are mostly distributed in band-like elongation to rolling or forging direction. The location in which carbides exist, is harder than other places in a component. The incompatibility of deformations between carbides and theirs neighbors leads to plastic zones even when cyclic loading is smaller than the yield limit of material at macro scale. The matrix region

around cleavage carbides during the application of cutting tools becomes a driving force for short crack growth under cyclic loading. In conclusion, broken carbides initiated micro-cracks and under cyclic loading these cracks continue to grow in the matrix phase until final fracture of the component [5, 20].

McDowell [18] originally developed a model, called multistage fatigue model (MSF). This model can completely describe the mechanisms of fatigue crack growth in metals (i.e. from nucleation stage to final failure). According to this model, fatigue crack growth can be divided into fourth stages: incubation, microstructurally small crack (MSC) and physically small crack (PSC), and long crack (LC) growth. Sometimes MSC is combined with PSC to form a unique stage named short crack growth. Based on this division, the total fatigue life N_T as shown in Eq.(1).

$$N_T = N_{inc} + N_{msc} + N_{psc} + N_{lc} \tag{1}$$

where N_{inc} is the number of cycles to incubate a micro notch scale crack with the length, a_{inc}, of the order of the carbide diameter. N_{msc} is the number of cycles required for propagation of a microstructurally short crack (MSC) with crack length in the range of $a_i < a < k \cdot GS$ (GS is the grain size), where k= 2-4. N_{psc} is the number of cycles required for propagation of a physically short crack (PSC) during the transition from MSC to that of a dominant long crack, and N_{lc} is the number of cycles during a long crack propagation (LC). In high strength steel, Lal [14] investigated that there is no transition phase from MSC to LC. That means MSC and PSC can be combined in term of short crack growth.

The fatigue crack initiation life of a component is the sum of the crack incubation and the short crack propagation life up to a predefined crack length, in general case $\leq 100\mu$m. In theory as well as experimental observation, the initiation life occupies about 90-98% in HCF [24]. For that reason, the prediction of fatigue crack initiation is a great significant. Based on this definition, fatigue crack initiation in forged M3:2 tool steel can be estimate:

$$N_i = N_{inc} + N_{sc} \tag{2}$$

in which N_i is the number of cycles to fatigue crack initiation and N_{sc} is number of cycles to short crack growth.

In McDowell's model [18], fatigue crack incubation is calculated by using the relationship between the Fatemi-Socie (F-S) damage parameter [7] and the Manson-Coffin law [6, 17], then fatigue crack incubation life can be calculated by FEM simulation. Whereas, short crack growth stage is described by Elasto-plastic Fracture Mechanics (EPFM). In this study, the calculation of short crack stage is developed by using the Lemaitre model [15]. The application of continuum damage mechanics (CDM) could be a promising approach. Consequently, both fatigue crack incubation and short crack growth are predicted by finite element analysis (FEA) at micro-meso scale.

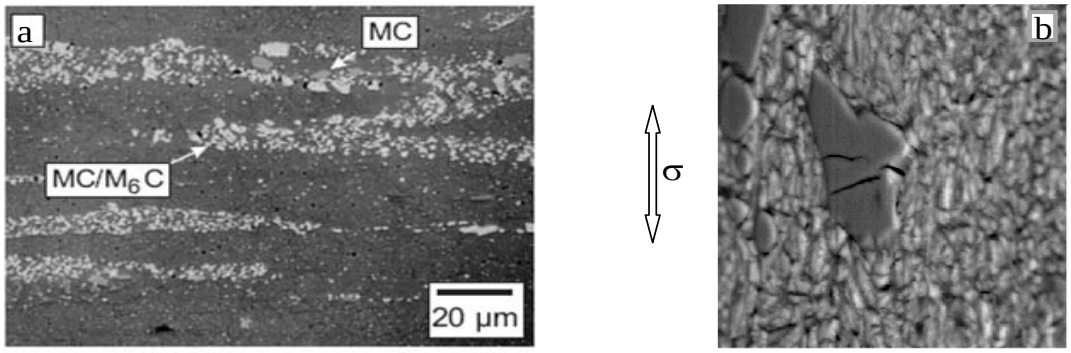

Figure 1: a) Microstructure of forged M3:2 [1], b) Crack initiation from a large primary carbide [19]

2 MATERIALS

Forged M3:2 tool steel is a classical M type Molybdenum rich tool steel. Since the manufacturing process involves forging, the tool steel contains a high amount of fine carbides, but a large number of broken primary and eutectic carbides also exist. The micrograph in Fig.1a) shows the primary and eutectic carbides which are distributed in a band-like structure. Fig.1b) presents the crack formation and propagation pattern during a component subjected to an external load. Cracks first appear in large primary and eutectic carbides (MC and M_6C) then grow in other parts of the material [19]. Fredriksson [8], studying crack growth in cold work steels, showed that fatigue cracks are initiated at larger primary carbides near or on the surface of specimens. Considering this particular case, a 2D model was used for the simulation of fatigue crack initiation.

2.1 Material model

Table 1: Mechanical properties of carbides and martensite of forged M3:2 tool steel [4, 19].

Phase	E [GPa]	ν [-]	σ_y^0[MPa]	σ_{ult} [MPa]	H [GPa]	σ_∞ [MPa]	b
MC and M_6C	400	0.25	-	1640	-	-	-
Martensite	210	0.3	987	-	30.0	417	137

At the micro-scale forged M3:2 tool steel is composed of two phases, the hard phase is primary and eutectic carbides and the soft phase is the martensite. Mishnaevsky [19], studying crack growth in high speed tool steel M3:2, generated a representative volume element (RVE) model with carbides distributed as band-like structure embedded in a martensitic steel matrix. Prasannavenkatesan [21], simulating microstructure effect on fatigue of heat treated and shot peened martensitic gear steel, modeled a martensitic steel matrix with nonlinear kinematic hardening. Consequently, for simplicity the carbide phase can be considered as an isotropic and elastic body and the martensite is a homogenous

and elasto-plastic continuum.

In this research, the combination of nonlinear isotropic hardening and linear kinematic hardening is performed, which is also coupled with CDM parameter by VUMAT subroutine in ABAQUS/EXPLICIT [11]. This approach might be a useful tool for describing the crack growth at micro-meso scale in cyclic loading. The summary of mechanical properties for both phases are given in Tab.1. Note that Tab.1, σ_y^0 is initial yield strength, σ_∞ is stabilization value of flow stress, H is the kinematic hardening modulus and σ_{ult} is ultimate tensile strength. Flow stress corresponding to nonlinear isotropic hardening of martensitic steel matrix is expressed

$$\sigma_{iso} = \sigma_y^0 + \sigma_\infty \left(1 - e^{-b\bar{\varepsilon}_{pl}}\right) \tag{3}$$

equivalent plastic strain increment is calculated

$$\Delta\bar{\varepsilon}_{pl} = \sqrt{\frac{2}{3}\Delta\boldsymbol{\varepsilon_{pl}} : \Delta\boldsymbol{\varepsilon_{pl}}} \tag{4}$$

Damage variable increment is defined as found in [25, 16]

$$\Delta D = \frac{D_c}{\varepsilon_R - \varepsilon_D} \cdot \left[\frac{2}{3}(1+v) + 3(1-2v) \cdot \left(\frac{\sigma_H}{\sigma_{eq}}\right)^2\right] \cdot \bar{\varepsilon}_{pl}^{2m} \cdot \Delta\bar{\varepsilon}_{pl} \tag{5}$$

in Eq.(5), σ_H is hydrostatic stress, σ_{eq} is von Mises stress and D is damage parameter whose value is bounded in $[0, 1]$. The damage constants, D_c, ε_R, ε_D and m are generally determined from loading-unloading tensile test. For the martensitic matrix, the constants were obtained from Wu's work [25] in which $D_c = 0.18, \varepsilon_R$=0.42, ε_D=0.01 and m=0.11.

The increment of back stress based on linear kinematic hardening law of martensitic steel matrix is performed

$$\Delta\boldsymbol{\alpha} = (1 - D)H\Delta\boldsymbol{\varepsilon_{pl}} \tag{6}$$

where $\boldsymbol{\alpha}$ is the back stress tensor and $\boldsymbol{\varepsilon_{pl}}$ is the platic strain tensor.

2.2 Micro-mechanical approach

Crack incubation and short growth are observed in a noncontinuous region due to the presence of carbides which cause stress concentration in cyclic plastic zones. The objective of simulation is to determine the time of the fatigue crack initiation. In this study, 2D RVE models were generated by capturing image information from SEM [26] in Fig.2, which is typical microstructure features of forged high speed tool steel; then typical microstructure features along with their mechanical properties given in Tab.1 of forged M3:2 tool steel were assigned. Element type is a plane stress element (CPS4R). The boundary conditions were applied in the RVE model from Jia [12], which satisfies the periodic homogeneous theory, illustrated in Fig.2.

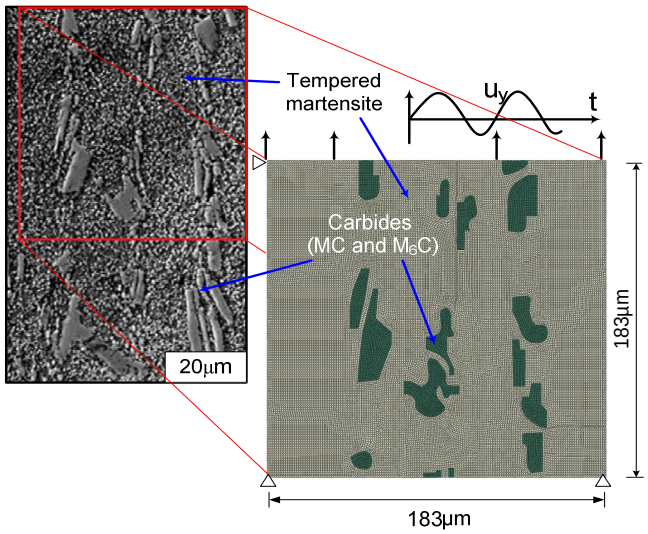

Figure 2: An RVE model generated according to SEM extracted from [26] for forged M3:2 and periodic boundary conditions (PBCs) for finite element analysis (FEA)

3 SIMULATION OF FATIGUE CRACK INITIATION

3.1 CDM approach

Models based on the degradation of the stiffness matrix or CDM could be a good solution in order to model and simulate fatigue nucleation and propagation in the matrix phase. Bonora et al.[3] developed CDM for crack propagation under cyclic loading. The criterion for crack propagation was based on plastic strain criterion. The relationship between the damage parameter increment and number of cycles to failure was determined during the simulation process. When using this model, plastic deformation would take into account during the fatigue life simulation.

• **Constitutive equations**

The combination of linear kinematic hardening and nonlinear isotropic hardening law in von Mises yield criterion coupled with CDM model was suitable approach for simulating crack growth under cyclic loading. The constitutive equation for the binder phase is performed

$$\phi((\mathbf{s}-\boldsymbol{\alpha}),\sigma_{iso}) = \sigma_{eq} - (1-D)\cdot\sigma_{iso} = \sqrt{\frac{3}{2}\cdot(\mathbf{s}-\boldsymbol{\alpha}):(\mathbf{s}-\boldsymbol{\alpha})} - (1-D)\cdot\sigma_{iso} \tag{7}$$

The strain increment in small time increment Δt is divided into two parts including $\Delta\boldsymbol{\varepsilon}_{el}$-elastic part and $\Delta\boldsymbol{\varepsilon}_{pl}$-plastic part as in Eq.(8)

$$\Delta\boldsymbol{\varepsilon} = \Delta\boldsymbol{\varepsilon}_{el} + \Delta\boldsymbol{\varepsilon}_{pl} \tag{8}$$

Generalized Hook's law is writen

$$\Delta\boldsymbol{\sigma} = (1-D)\cdot(\lambda trace(\Delta\boldsymbol{\varepsilon}_{el})\mathbf{I} + 2\mu\Delta\boldsymbol{\varepsilon}_{el}) \tag{9}$$

where λ and μ are Lame constants.

Plastic flow rule:

$$\Delta\boldsymbol{\varepsilon}_{pl} = \Delta\boldsymbol{\gamma}\cdot\mathbf{Q} \tag{10}$$

in which $\Delta\boldsymbol{\gamma}$-plastic multiplier which was determined from return mapping method when simulating. $\mathbf{Q}$ is unit normal to the yield surface. $\mathbf{Q}$ is defined $\mathbf{Q} = \frac{\mathbf{s}-\boldsymbol{\alpha}}{\|\mathbf{s}-\boldsymbol{\alpha}\|}$. In above equations, $\mathbf{s}$-deviatoric stress, $\mathbf{s} = \boldsymbol{\sigma} - \sigma_m\mathbf{I}$ in which $\boldsymbol{\sigma}$-Cauchy stress and $\sigma_m = \frac{1}{3}\text{trace}(\boldsymbol{\sigma})$.

• Stress integration algorithm

Assuming that the values of the state internal variables such as the damage indicator D_{t_n}, Cauchy stress $\boldsymbol{\sigma}_{t_n}$, equivalent plastic strain $\Delta\bar{\varepsilon}_{pl,t_n}$ and the strain increment $\Delta\boldsymbol{\varepsilon}_{t_n}$ were known at the time t_n.

At the beginning, assuming that the strain is completely elastic strain, i.e. $\Delta\boldsymbol{\varepsilon}_{pl} = 0$. Thus, generalized Hook's law is calculated

$$\Delta\boldsymbol{\sigma}_{trial} = \Delta\boldsymbol{\sigma}_{t_n} + (1-D_{t_n})\cdot(\lambda trace(\Delta\boldsymbol{\varepsilon})\mathbf{I} + 2\mu\Delta\boldsymbol{\varepsilon}) \tag{11}$$

where $\Delta\boldsymbol{\sigma}_{trial}$-trial stress (called elastic predictor)

Therefore, the trail deviatoric stress can be computed as

$$\mathbf{s}_{trial} = \boldsymbol{\sigma}_{trail} - \frac{1}{3}trace(\boldsymbol{\sigma}_{trail})\mathbf{I} \tag{12}$$

and the translation of the yield surface

$$\boldsymbol{\xi}_{trial} = \boldsymbol{\sigma}_{trail} - \frac{1}{3}trace(\boldsymbol{\sigma}_{trail})\mathbf{I} \tag{13}$$

substituting the $\mathbf{s}_{trial}$ into yield function $\phi((\mathbf{s}-\boldsymbol{\alpha}), \sigma_{iso})$, if $\phi((\mathbf{s}-\boldsymbol{\alpha}), \sigma_{iso}) < 0$ the elastic deformation assumed is true. State variables are updated at the time t_{n+1}

$$\begin{aligned}
\boldsymbol{\sigma}_{t_{n+1}} &= \boldsymbol{\sigma}_{trail} \\
\bar{\boldsymbol{\varepsilon}}_{pl,t_{n+1}} &= \bar{\boldsymbol{\varepsilon}}_{pl,t_n} \\
D_{t_{n+1}} &= D_{t_n}
\end{aligned} \tag{14}$$

If $\phi((\mathbf{s}-\boldsymbol{\alpha}), \sigma_{iso}) > 0$, the yield surface has been expanded during time increment Δt and the translation of the yield surface is described:

$$\boldsymbol{\xi}_{t_{n+1}} = \mathbf{s}_{t_{n+1}} - \boldsymbol{\alpha}_{t_{n+1}} \tag{15}$$

In order to satisfy the compatible condition during yield surface expanding, $\mathbf{s}_{t_{n+1}}$ must be lied on the yield surface, i.e.,

$$\boldsymbol{\xi}_{t_{n+1}} = \mathbf{R}_{t_{n+1}}\mathbf{Q} \tag{16}$$

where $\mathbf{R}_{t_{n+1}}$ is the radius of yield surface at the time t_{n+1}. $\mathbf{R}_{t_{n+1}}$ is calculated as

$$\mathbf{R}_{t_{n+1}} = \sqrt{\frac{2}{3}} \cdot \left(1 - D_{t_{n+1}}\right) \cdot \sigma_{(iso,t_{n+1})} \tag{17}$$

Solving for plastic multiplier $\Delta\boldsymbol{\gamma}$ from Eq.(7), the state variables are updated at the time t_{n+1}

$$\begin{aligned}
\bar{\boldsymbol{\varepsilon}}_{pl,t_{n+1}} &= \bar{\boldsymbol{\varepsilon}}_{pl,t_n} + \sqrt{\frac{2}{3}}\Delta\boldsymbol{\gamma} \\
D_{t_{n+1}} &= D_{t_n} + \sqrt{\frac{2}{3}}\Omega_{t_n}\Delta\boldsymbol{\gamma} \\
\boldsymbol{\sigma}_{t_{n+1}} &= \boldsymbol{\sigma}_{trail} - 2\mu\Delta\boldsymbol{\gamma}\mathbf{Q} \\
\boldsymbol{\alpha}_{t_{n+1}} &= \boldsymbol{\alpha}_{t_n} + \sqrt{\frac{2}{3}}H\left(1 - D_{t_n}\right)\Delta\boldsymbol{\gamma}\mathbf{Q}
\end{aligned} \tag{18}$$

3.2 Simulation of fatigue crack incubation

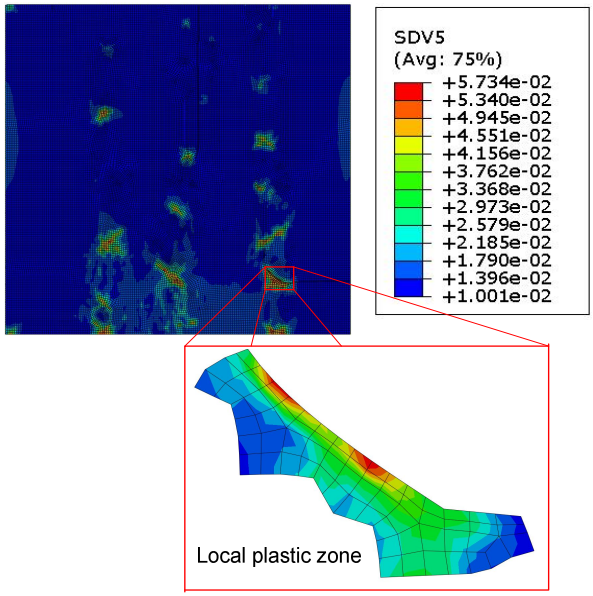

Figure 3: A local plastic zone in RVE model of forged M3:2 tool steel subjected by remote strain amplitude $\varepsilon_a = 0.4\%$

It is known that local plastic zones are the main factors causing fatigue crack incubation under cyclic loading. In this study, the hysteresis loop is stable after the 3^{rd} cycle; for the estimation of fatigue crack incubation, the stress and strain histories were analyzed at each Gauss points in the local plastic zone over the stabilization load cycle. Note that the non-local volume average for stress and strain histories can be calculated as follows.

$$\Sigma = \frac{1}{V_\Sigma} \int_{V_\Sigma} \Sigma^{'} dV \tag{19}$$

where Σ is the average parameter of $\Sigma^{'}$ over the local plastic zone whose area is bounded by the elements with equivalent plastic strain (SDV5) at element nodes over 0.01%, illustrated in Fig.3.

Thus, the Fatemi-Socie parameter, $\Delta\Gamma_{FS}$, is calculated based on multiaxial critical plane defined in Eq.(20)

$$\Delta\Gamma_{FS} = \frac{\Delta\gamma^{p*}_{\max}}{2}\left(1 + K^* \frac{\sigma_n^{max}}{\sigma_y^0}\right) \tag{20}$$

where the coefficient, K^*, takes into account the interaction of torsional and tension fatigue ductility, and lies in the range of 0.5 to 1. In this study, K^* was chosen to be 1. $\frac{\Delta\gamma^{p*}_{\max}}{2}$ is maximum plastic shear strain range on critical plane in the local plastic zone and σ_n^{max} is normal stress on this plane.

Number of cycles to fatigue crack incubation is calculated by the relationship between Manso-Coffin law and Fatemi-Socie parameter as following

$$\Delta\Gamma_{FS} = \frac{\Delta\gamma^{p*}_{\max}}{2}\left(1 + \frac{\sigma_n^{max}}{\sigma_y^0}\right) = C_{inc}(2N_{inc})^{\eta} \tag{21}$$

in Eq.(21), where η and C_{inc} are material dependent parameters determined for forged M3:2 tool steel given in [9, 10]: C_{inc}=0.56 and η =-0.407.

3.3 Simulation of short crack growth

The short crack growth in forged M3:2 tool steel using CDM was implemented by VUMAT subroutine in ABAQUS/EXPLICIT. The crack path is established by deleting element which has damage parameter (SDV7) is greater than D_c, illustrated in Fig.4. The result shows that crack originates from a large carbide near the edge of the RVE, which is in good agreement with Randelius' conclusion [22].

Note that since the crack length is within RVE dimension, it could be considered as short crack. Consequently, the number of cycle to short crack growth is predicted based on simple equation suggested by Redl et al. [23] and Krumphals et al. [13] as follows

$$N_f = \frac{1}{\Delta D_S} \tag{22}$$

where ΔD_S is damage parameter increment within a stabilization cycle, in this research $\Delta D_S = \Delta D_3$.

Thus, number of cycles to short crack growth in forged M3:2 tool steel are computed in Eq.(23) over the 3^{rd}cycle.

$$N_{sc} = \frac{1}{\Delta D_3} \tag{23}$$

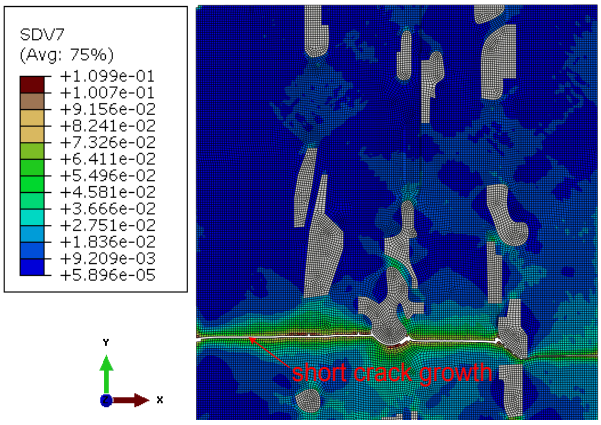

Figure 4: Short crack growth in RVE model of forged M3:2 tool steel subjected by remote strain amplitude $\varepsilon_a = 0.4\%$

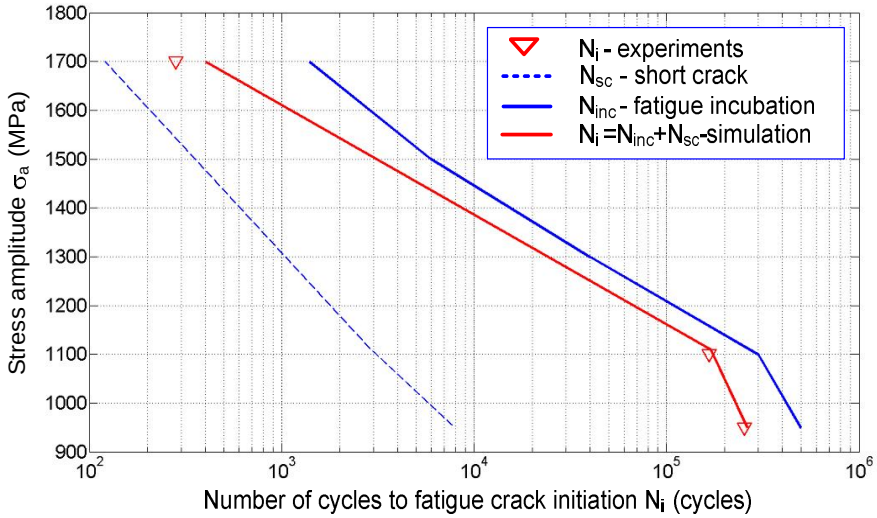

Figure 5: Comparison of fatigue crack initiation of simulation and experiment in forged M3:2

4 RESULTS AND DISCUSSION

Number of cycles to fatigue crack initiation is defined in Eq.(24)

$$N_i = N_{inc} + N_{sc} \tag{24}$$

The simulation results with remote strain loading amplitude varies $\varepsilon_a = 0.3 - 0.8\%$ corresponding to stress amplitude $\sigma_a = 980 - 1700$ MPa were compared to those of experiment of forged M3:2 tool steel in [2]. These comparisons are illustrated in Fig.5 which show that the prediction model can be considered proper because the deviation is in a slightly comparable range.

5 CONCLUSIONS

- The CDM was developed for predicting fatigue crack initiation (i.e. formation plus short crack growth) in forged M3:2 tool steel. The results of simulation for predicting fatigue crack initiation seem appropriate with those from fatigue experiments. Thus, this approach provides another method beside existing methods for simulating fatigue crack initiation in tool steels.

- A simple framework was introduced for calculating initiation lifetime of forged M3:2 tool steel by using VUMAT subroutine in ABAQUS/EXPLICIT.

REFERENCES

[1] Berns, H., Broeckmann, C., and Hinz, H. F. Creep of high speed steels, Part I-experimental investigation. In *6th International tooling conference* (Karlstad, Sweden, 2002), pp. 325–348.

[2] Berns, H., Lueg, J., Trojahn, W., Waehling, R., and Wisell, H. Fatigue behavior of conventional and powder metallurgical high speed steel. *Powder metallurgy international 19* (1987), 22–26.

[3] Bonora, N. A nonlinear CDM model for ductile failure. *Enginering Fracture Mechanics 58* (1997), 11–28.

[4] Broeckmann, C. *Kriechen partikel-verstaerkter metallischer Werkstoffe.* VDI Verlag GmbH, Duesseldorf, Germany, 2001.

[5] Broeckmann, C., Packeisen, A., and Theisen, W. Fatigue of carbide rich materials. In *7th International tooling conference* (Torino, Italy, 2006), pp. 3–12.

[6] Coffin, L. F. J. A study of the effects of cyclic thermal stresses on a ductile metal. *Transactions of the American Society of Mechanical Engineers 76* (1954), 931–950.

[7] Fatemi, A., and Socie, D. A critical plane approach to multiaxial fatigue damage including out-of-phase loading. *Fatigue Fracture Eng. Mater. Struc. 11*, 3 (1988), 145–165.

[8] Fredriksson, G., Bergstroem, J., and Hogmark, S. Crack growth in cold work tool steels-influence of surface condition, microstructure and hardness. In *6th International tooling conference* (Karlstard, Sweeden, 2002), pp. 125–135.

[9] Giang, N. A., Bezold, A., and Broeckmann, C. Simulation of fatigue crack incubation of casted/forged HS6-5-3 tool steel under HCF regime. In *3rd Fatigue Symposium* (Leoben, Austria, 2012), pp. 6–25.

[10] Giang, N. A., Oezden, U. A., Bezold, A., and Broeckmann, C. A model for predicting crack initiation in forged M3:2 tool steel under high cycle fatigue. *International Journal of Fracture 187* (2014), 145–158.

[11] Hibbitt, H. D., Karlsson, B. I., and Sorensen, E. P. *ABAQUS-Standard, User Manual, Version 10.1.* Inc. Pawtucket RI, USA, 2011.

[12] Jia, S., and Povirk, G. L. Modelling the effects of reinforcement distribution on the elastic properties of composite materials. *Modelling Simul. Mater. Sci. Eng. 6* (1998), 587–602.

[13] Krumphals, F., Wlanis, T., Sievert, R., Wieser, V., and Sommitsch, C. Damage analysis of extrusion tools made from the austenitic hot work tool steel Böhler W750. *Computational Materials Science* (2010), 1–6.

[14] Lal, D. N. The influence of strength and stress ratio on short-crack thresholds and non-propagating fatigue crack. *Fatigue of Engineering Materials and Structures 16* (1993), 419–428.

[15] Lemaitre, J. *A course on damage mechanics.* Springer-Verlag, Berlin, Germany, 1996.

[16] Li, H., Fu, M. W., Lu, J., and Yang, H. Ductile fracture: experiments and computations. *International Journal of Plasticity 27* (2011), 147–180.

[17] Manson, S. S. Behaviour of materials under conditions of thermal stress. Technical report NACA-TR-1170, National Advisory Commission on Aeronautics, 1954.

[18] McDowell, D. L., Gall, K., Horstemeyer, M., and Fan, J. Microstructure-based fatigue modeling of cast A356-T6 Alloy. *Engineering Fracture Mechanics 70* (2003), 49–80.

[19] Mishnaevsky, J. L., Lippmann, N., and Schmauder, S. Mico-mechanisms and modelling of crack initiation and growth in tool steels: role of primary carbides. *Z.Metallkd 94* (2003), 676–681.

[20] Picas, I. *Mechanical behaviour of tools for shearing Ultra High-Strength Steels: influence of the microstructure on fracture and fatigue micro-mechanisms of tool steels and evaluation of micro-mechanical damage in tools.* Ph.D. thesis, Universitat Politecnica de Catalunya, Spain, 2012.

[21] Prasannavenkatesan, R. *Microstructure-sensitive fatigue modeling of heat treated and shot peened martensitic gear steels.* Ph.D. thesis, Georgia Institute of Technology, USA, 2009.

[22] Randelius, M. Influence of microstructure on fatigue and ductility properties of tool steels. Master's project, Materials Science and Engineering, Royal Institute of Technology, Sweden, 2008.

[23] Redl, C., Wieser, V., Sommitsch, C., Schuetzenhefer, T., Gaudin, S., and Geigges, B. Investigation and numerical modeling of extrusion tool life time. In *7th International tooling conference* (Torino, Italy, 2006), pp. 589–595.

[24] Wang, Q. Y., Berard, J. Y., Rathery, S., and Bathias, C. High cycle fatigue crack initiation and propagation behavior of high-strength spring steel wire. *Fatigue Fract. Engng. Mater. Struct. 22* (1999), 673–677.

[25] Wu, T. *Experiment and numerical simulation of welding induced damage stainless steel 15-5PH.* Ph.D. thesis, Devant Linstitut national des sciences appliquees de Lyon, France, 2007.

[26] Zhou, X., Yin, X., Fang, F., and Jiang, J. Effect of calcium modification on the microstructure and properties of high speed steel. *Advanced Materials Research 217–218* (2011), 457–462.